Journal of Environmental Management 375 (2025) 124426

Contents lists available at ScienceDirect

Journal of Environmental Management

journal homepage: www.elsevier.com/locate/jenvman

Research article

Engineering cement-free high-performance Martian concrete with enhanced in-situ utilization of soil simulant: Curing across −20 °C–40 °C and CO_2-rich environments

Ruizhe Shao [a], Chengqing Wu [b,a,*], Jun Li [a]

[a] School of Civil and Environmental Engineering, University of Technology Sydney, Sydney, NSW, 2007, Australia
[b] Institute of Rock and Soil Mechanics, Chinese Academy of Sciences, Wuhan, 430071, China

ARTICLE INFO

Keywords:
High-performance Martian concrete
Martian soil simulant
In-situ resource utilization
Fibre reinforcement
Martian environment
Compression performance
Microstructure

ABSTRACT

Mars is increasingly considered for colonization by virtue of its Earth-like conditions and potential to harbor life. Responding to challenges of the Martian environment and the complexity of transporting resources from Earth, this study develops a novel geopolymer-based high-performance Martian concrete (HPMC) using Martian soil simulant. The optimal simulant addition, ranging from 30% to 70% of the total mass of the binders, was explored to optimize both the performance of HPMC and its cost-effectiveness. Additionally, the effects of temperature (−20 °C–40 °C) and atmospheric (ambient and carbonated) curing conditions, as well as steel fibre addition, were investigated on its long-term compressive and microstructural performance. Optimal results showed that HPMC with 50% regolith simulant achieved the best 7-day compressive strength (62.8 MPa) and the remarkable efficiency improvement, a result of ideal chemical ratios and effective geopolymerization reaction. Under various temperature conditions, sub-zero temperatures (−20 °C and 0 °C) diminished strength due to reduced aluminosilicate dissolution and gel formation. In contrast, specimens cured at 40 °C and 20 °C, respectively, showed superior early and long-term strengths, with the 40 °C potential for moisture loss related shrinkage cracking and reduced geopolymerization. Regarding the atmospheric environment, carbonation curing and steel fibre addition both improved the matrix compactness and compressive strength, with carbon-cured fibre-reinforced HPMC achieving 98.3 MPa after 60 days. However, long-term exposure to high levels of CO_2 eventually reduced the fibres' toughening effect and caused visible damages on steel fibres.

1. Introduction

The relentless pursuit of human space exploration has increasingly targeted Mars, the closest planet with Earth-like conditions, as a pivotal outpost for extending humanity's reach beyond Earth. Given its proximity and potential to support life, Mars is poised to become an ideal destination for human colonization (Levchenko et al., 2021). Both global public and private space agencies aim to establish a human settlement on Mars by 2050 (Scott et al., 2017). This endeavour is driven not only by the excitement of discovering new worlds but also by practical considerations of long-term survival and scientific progress.

To facilitate further exploration and eventual colonization on Mars, the establishment of a Martian base serves as a critical and foundational step (Szocik et al., 2020; Neukart, 2024). This base provides a secure hub for operations and a robust platform for conducting essential scientific research, thereby underpinning sustainable human habitation on Mars. However, constructing such a base poses notable challenges, including the vast interplanetary distance, the thin Martian atmosphere, and frequent dust storms on its surface. The elevated costs associated with transporting materials from Earth to Mars underscore the urgent need for innovative and sustainable solutions. Against this backdrop, the strategy of in-situ resource utilization (ISRU) (Shao et al., 2024, 2025; Wu et al., 2024a; Scott et al., 2020) becomes indispensable. ISRU significantly mitigates the need to transport the terrestrial materials, therefore reducing costs and enhancing the feasibility of sustainable, self-sufficient operations on Mars, which are vital for prolonged colonization efforts.

Concrete is a fundamental material in terrestrial construction, valued for its exceptional compressive strength, high durability, and a wide range of strength gradations. Recognizing the extensive use of concrete

* Corresponding author. Institute of Rock and Soil Mechanics, Chinese Academy of Sciences, China.
E-mail addresses: Ruizhe.shao@uts.edu.au (R. Shao), Cqwu@whrsm.ac.cn (C. Wu), Jun.li-2@uts.edu.au (J. Li).

https://doi.org/10.1016/j.jenvman.2025.124426
Received 1 October 2024; Received in revised form 11 January 2025; Accepted 31 January 2025
Available online 4 February 2025

on Earth, McKay et al. (1996) introduced the concept of Martian concrete in 1996, suggesting that the acquisition of essential raw materials for concrete production on Mars would be relatively straightforward. This viewpoint therefore supported the feasibility of Martian concrete as a practical building material for infrastructure on Mars. At present, research on Martian concrete is becoming increasingly marked in the field of extra-terrestrial construction, leading to the proposal of a variety of concrete formulations and methodologies (Scott et al., 2020; Reches, 2019; Wan et al., 2016; Akono, 2023; Shahsavari et al., 2022; Mills et al., 2022). For example, Scott et al. (2020) synthesized a Martian concrete by combining a magnesium silica (MS) binder with various Martian soil simulants sourced from New Zealand. Their study revealed that the MS hydrate produced a mixture with high viscosity, which potentially impeded the escape of entrapped air during compaction. This behaviour led to increased porosity and reduced compressive strength. However, despite these challenges, the air-cured method achieved a commendable 90-day compressive strength of around 35.5 MPa with a water-cement ratio of 0.4. In their another research (Scott and Oze, 2018), it was discovered that olivine, a mineral abundantly found on Mars, along with its hydrolysis products (such as $MgCO_3$) produced molecular hydrogen. This reaction presented a potentially viable method for both concrete and fuel production on Mars, requiring minimal energy expenditure and primarily dependent on the availability of water. However, it is well established that the production of MS concrete necessitates a substantial volume of water (Gonçalves et al., 2020; Tran and Scott, 2017). Considering the scarcity of water on Mars, the alternatives such as sulphur concrete, which eliminates the need for water during its preparation, and geopolymer concrete, which exhibits almost zero reliance on water resources, are garnering increased attention from researchers.

Wan et al. (2016) conducted a detailed study into the effect of molten sulphur addition on the behaviour of Martian concrete, utilizing the soil simulant JSC-Mars-1A as the matrix aggregate. Their findings indicated that the aggregate size significantly affected the concrete final strength. Notably, a mixture containing 50% each of sulphur and simulant yielded the highest compressive and flexural strengths of more than 50.0 and 1.5 MPa, respectively. Additionally, the interaction between the rich metallic elements in the simulant and sulphur during the hot mixing at 120 °C was identified as a vital factor enhancing the strength of Martian concrete. Building on the optimum ratio of Martial simulant and sulphur proposed by Wan et al. (2016), Akono (2023) studied the effect of three simulants, designated as MGS-1. MGS-1S, and MMS-1, on the microstructure and fracture performance of Martian concrete. The results showed that the basic matrix of concretes had a Young's modulus ranging from 18.8 to 25.2 GPa and featured a microporous structure with 1–2 μm pitch sizes. In addition, these concretes exhibited a nonlinear fracture response with toughness values of approximately 0.48 (MMS-1) and 0.75 MPa $m^{0.5}$ (MGS-1 and MGS-1S). In terms of the geopolymer-based Martian concrete, Mill et al. (Mills et al., 2022) activated the soil simulant MGS-1C with an alkaline sodium silicate solution under various conditions, including ambient curing and exposure to temperatures of 600 and -80 °C. The findings revealed that the 7-day compressive strength of mixtures cured in ambient conditions reached up to 13.6 MPa. However, this strength diminished to 1.5 and 12.2 MPa following sub-zero and extreme high temperature exposures, respectively, likely due to the lower iron and magnesium content in the simulant. Leveraging progresses in 3D printing technology, Ma et al. (2022) developed a geopolymer ink composed of basalt fibre-reinforced Martian simulant HIT-MRS-1 for use in direct ink writing. This ink exhibited superior rheological properties, enabling the swift transition from solid to liquid that improved the printability of geopolymers with customizable biomimetic patterns. Notably, the helical pattern achieved the highest compressive strength of 32.2 MPa, whereas the suture pattern, with a lower strength of 9.3 MPa, showed high fracture ductility suitable for deformation-resistant materials. Further contributions to this field were made from Vitse et al. (2024) and Karacasulu et al. (2023), who independently developed MGS-1-based geopolymer concrete with compressive strengths of approximately 30.5 and 42.5 MPa, respectively. Compared with the traditional sulphur concrete, geopolymer composites present several advantages critical for Martian applications. These include enhanced heat resistance, improved chemical durability, superior resistance to temperature cycling, and increased vacuum stability (Panda et al., 2024; Xu et al., 2023; Wang et al., 2016; Yang et al., 2024). Besides, another significant benefit of geopolymer concrete is its utilization of the abundant aluminosilicate-rich Martian regolith (McSween and Keil, 2000; Fackrell et al., 2021). This is coupled with the potential exploitation of water resources on Mars (Nazari-Sharabian et al., 2020; Orosei et al., 2018), which are important not only for the formation of geopolymer binders but also facilitate its chemical synthesis processes. Unlike sulphur concrete, geopolymers do not require high-temperature treatment, leading to a significant reduction in the energy consumption for construction activities on Mars. Given these remarkable advantages, several researchers advocated for the use of geopolymer-based concrete as the optimal material for construction activities on Mars (Wu et al., 2024a; Iranfar et al., 2023; Zamani et al., 2024).

Deep space exploration and Martian base development represent cutting-edge areas in the scientific research. A vital aspect of these endeavours involves utilizing indigenous resources, particularly for producing Martian concrete. Despite the progress, current methodologies for the prepared Martian concrete remain nascent, with materials exhibiting suboptimal behaviour across several properties essential for withstanding the harsh conditions of Mars. Given severe temperature fluctuations and the predominantly carbon dioxide atmosphere, there is a pressing need for concrete that possesses both enhanced strength and durability (Hu et al., 2022). In response to these challenges, this study introduces an innovative formulation for high-performance Martian concrete (HPMC), focusing on the impacts of varying regolith simulant proportions on its early-age performance and cost-efficiency. Besides, this research explores a variety of temperature and atmospheric curing methods, as well as the inclusion of steel fibre reinforcement, to assess their effects on the long-term compression and microstructural characteristics of the concrete. The advancements achieved herein are vital for improving ISRU on Mars, thus supporting the long-term sustainability of human activities on the Red Planet.

2. Experimental programs

2.1. Raw materials

Due to the unavailability of actual Martian soil for experimental purposes, the Mars Global Simulant (MGS-1) was used in this study to synthesize geopolymer-based HPMC. MGS-1 is a commercially available synthetic compound procured from Space Resource Technologies (SRT) and specifically designed to replicate the mineralogical composition of Martian regolith, particularly the soil at Gale Crater Rocknest site (Cannon et al., 2019). This design is based on analyses conducted by various Mars missions and orbital studies. The simulant incorporates a crystalline fraction, an amorphous fraction, oxychlorines, nitrates, and a representative bulk chemistry.

The primary constituents of MGS-1 include silica, magnesium, iron, aluminium, and calcium, which collectively constitute over 90% of its oxide composition, as detailed in Table 1. The median particle size of MGS-1 is recorded at 63 μm, and its angles of repose average at 38.9° and peak at 43.6°. Fig. 1 shows the micromorphology and mineralogical phases of MGS-1, revealing distinct morphologies: polyporous cylinder olivine, angular bytownite, and smooth, irregular anorthosite. The predominant mineral phases identified are anorthite, bytownite, albite high, and olivine, all displaying significant hump intensity, consistent with observations reported in the reference (Snehal et al., 2024). It is noteworthy that the partial dissolution of feldspars phases in MGS-1, such as anorthite and albite, under highly alkaline conditions, facilitates the release of reactive aluminosilicates contributing to geopolymer

Table 1
Major bulk chemistry and physical attributes of aluminosilicate source materials.

Materials	Chemical oxide composition (wt. %)							Bulk density (kg/m^3)	LOI (%)	PSR (μm)
	SiO_2	Al_2O_3	CaO	Fe_2O_3	MgO	Na_2O	TiO_2			
MGS-1	43.9	12.8	7.9	10.6	14.8	1.5	0.4	1400	4.90	0.04–1000
Fly ash	65.2	24.7	1.6	4.3	1.2	0.3	0.9	1073	1.10	0.25–130
Silica fume	89.6	2.1	1.9	1.5	0.8	0.4	<0.1	625	3.80	0.03–0.20
GGBFS	35.4	10.8	43.6	0.4	8.1	0.2	0.5	1275	0.48	0.20–100

Note: "LOI" denotes loss on ignition and "PSR" denotes particle size range parameter.

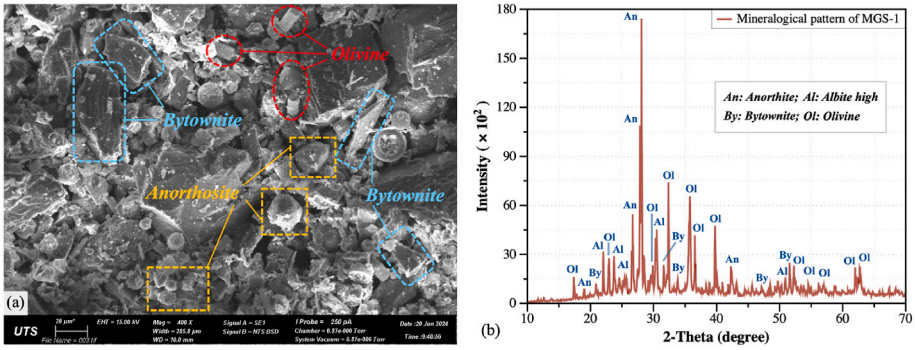

Fig. 1. (a) Micromorphology and (b) mineralogical phases of the incorporated MGS-1.

formation (González-et al., 2017; Nana et al., 2019). MGS-1's high fidelity as a basaltic soil simulant, combined with its robust characterization and proven ability to mimic the essential geopolymer precursors (Mills et al., 2022), underscores its dual utility in formulating HPMC as both a reactive binder component and a structural aggregate.

To augment the geopolymerization process and enhance the mechanical properties of the formulated geopolymers, an admixture of calcium-aluminium-silicate-rich materials, including silica fume, fly ash, and granulated blast-furnace slag (GGBFS), were incorporated. The major oxide composition and physical properties of these materials are also listed in Table 1, while their micromorphological patterns, observed under a Scanning Electron Microscope (SEM) apparatus, are presented in Fig. 2. An alkaline solution comprising sodium silicate (Na_2SiO_3) and sodium hydroxide (NaOH) was used to initiate the geopolymerization of the aluminosilicate-bearing precursors. In addition, straight steel fibres, 10 mm in length and with a tensile strength exceeding 2500 MPa, were integrated to reinforce the concrete matrix. The fibres incorporated in HPMC mixtures possessed exceptional resistance to both alkaline and acidic conditions, which renders them highly suitable for environments prone to high corrosion.

In this experiment, geopolymer-based HPMC mixtures were formulated both with and without steel fibres, designated as HPMC-SF and HPMC-PL series, respectively. The constituents of these mixes are detailed in Table 2. Specifically, within the HPMC-PL series, variants MC-PL30, MC-PL50, and MC-PL70 corresponded to plain concrete mixtures in which Martian simulant constituted 30%, 50%, and 70% of the total mass of MGS-1, GGBFS, fly ash, and silica fume. Although increasing MGS-1 content changed the overall mass of GGBFS, fly ash, and silica fume, the ratios among these three supplementary precursor materials remained fixed. This fixed ratio was derived from prior research on developing the geopolymer-based ultra-high performance concrete (UHPC), which identified the optimal mix proportions for achieving robust mechanical properties (Xu et al., 2021). In contrast, the MC-SF0.6 variant within the HPMC-SF series involves a 0.6% steel fibre dosage, selected based on previous work with lunar concrete (Shao et al., 2025). Throughout all mixes, the mass of liquid components (alkaline solution + water) was standardized to a fiducial value, maintaining a solid-to-liquid mass ratio of 4.97:1.18. This design method provides a consistent chemical framework for comparing performance of HPMC across varying MGS-1 contents.

2.2. Preparation and curing

To formulate the geopolymer-based HPMC, Martian simulant and additional solid materials were initially dry blended utilizing a Hobart mixer for 3–5 min. For the preparation of fibre-reinforced geopolymers, steel fibres were uniformly dispersed into the dry mixture over a period of 1–2 min. An alkaline solution was then gradually incorporated into the mix over 3–4 min at a low blending speed. This was followed by the addition of the remaining water, with the mixing continued for an

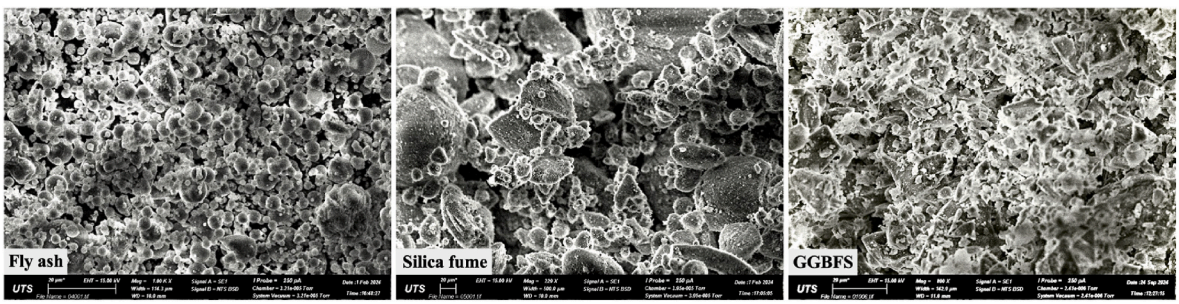

Fig. 2. Micromorphology of the incorporated precursor materials.

Table 2
Mixture constituents of synthesized HPMC by weight.

Group	Specimen	MGS-1	GGBFS	Fly ash	Silica fume	AAS	Water	Fibre (vol. %)
HPMC-PL	MC-PL30	1.49	2.76	0.44	0.28	1.00	0.18	0.0
	MC-PL50	2.49	1.97	0.31	0.20	1.00	0.18	0.0
	MC-PL70	3.48	1.18	0.19	0.12	1.00	0.18	0.0
HPMC-SF	MC-SF0.6	2.49	1.97	0.31	0.20	1.00	0.18	0.6

Note: "AAS" denotes alkali activator solution and "vol. %" denotes volume fraction of fibre dosage.

additional 2–3 min at a higher speed to achieve a homogeneous consistency. The mixtures were subsequently cast into plastic cubic moulds with dimensions of 50 × 50 × 50 mm. The moulds were vibrated for approximately 25 s to eliminate air pockets. Following this, the mixtures within the moulds were covered with polyethylene films to prevent water evaporation and were left to cure in ambient conditions for 24 h to achieve initial strength.

After the specimens were demoulded 24 h post-casting, different curing regimes were adopted for various concrete series as shown in Table 2. Specifically, the HPMC-PL series was subjected to ambient curing at 20 °C to establish the optimal MGS-1 addition for Martian concrete. Subsequently, both plain and fibre-reinforced (HPMC-SF case) Martian concrete specimens, based on this optimal simulant percentage, were casted, demoulded, and subjected to diverse temperature and atmospheric conditions for 7, 28, and 60 days to evaluate their performance within the Martian-like environments. The temperature conditions tested included −20 °C, 0 °C, 20 °C, and 40 °C. The selection of −20 °C and 40 °C was based on the lowest operational temperature of the laboratory freezer and the highest temperature recorded near the Martian equator (Snehal et al., 2024), respectively. Atmospheric conditions examined were ambient air and a carbonation process. The latter was specifically chosen due to the high CO_2 concentration (over 95%) in the Martian atmosphere (Triaud et al., 2024). It is important to note that the simulated carbonation environment in the laboratory did not achieve the identical CO_2 concentrations as those of Mars. However, the use of vacuum-sealed chambers with continuous CO_2 gas injection ensured that the CO_2 concentration within chambers consistently exceeded 90%. The preparation and curing processes for the HPMC specimens are schematically depicted in Fig. 3.

2.3. Testing methods

The flowability and setting time of the fresh HPMC mixture were evaluated immediately following mixing, in accordance with ASTM C1437 (ASTM C1437, 2013) and ASTM C191 (ASTM C191, 2013). Mechanical properties of the resulting geopolymer pastes, specifically the compressive strength, were evaluated at 1, 7, 28, and 60 days post-curing employing diverse curing regimes. These tests were conducted in compliance with ASTM C109/C109M (ASTM C109 et al., 2013) utilizing a state-of-the-art servo-hydraulic universal testing machine (UTM UH-500, Australia). The loading rate was maintained at 0.1 mm/min to delineate the complete stress-strain relationships for the specimens under examination.

Meanwhile, a Digital Image Correlation (DIC) system was operational, matching the data collection frequency of the UTM to monitor the strain distribution and the progression of failure within HPMC specimens. To ensure the reliability of the test outcomes, three identical specimens were evaluated, and their average values were used to represent the ultimate compressive strength. Furthermore, the hardened density of each concrete mixture was determined via measuring the cubic mass of batch-consistent HPMC specimens prior to the mechanical testing.

Following the completion of the destructive mechanical tests, intact pieces and the corresponding ground powder collected from the damaged concrete fragments were subjected to detailed analyses. These analyses aimed to characterize the phase identification, hydration products, micromorphology, and element distribution across varying mixture proportions under different curing conditions. The advanced instrumentation, including a Zeiss EVO LS15 SEM paired with RaithElphy Lithography Energy Dispersive Spectroscopy (EDS), and a Bruker D8 Discover X-ray Diffraction (XRD) system, was employed.

3. Results and discussion

3.1. Effect of simulant content

3.1.1. Fresh mixture performance

The fresh performance of geopolymer-based HPMC is crucial for ensuring its mechanical properties, structural performance, and durability. Fig. 4(a) displays the changes in slump flowability of HPMC with varying MGS-1 contents. A linear increase in flow diameter from 30% to 70% MGS-1 content is prominent, with a strong correlation coefficient ($R^2 = 0.987$). Specifically, flowability percentages rose from 92.2% to 110.8% and further to 133.3% with increasing MGS-1, highlighting enhanced flowability performance of HPMC. Additionally, Fig. 4(b) shows the impact of MGS-1 content on the setting time of HPMC, assessed utilizing a Vicat needle. With 30% MGS-1, the initial and final setting times were 21 and 29 min, respectively - an extension of 38.1%. This extension increased to 53.1% for 50% MGS-1 content (32 min initial, 49 min final), and further to 62.2% for 70% MGS-1 content (45 min initial, 73 min final). These setting time variations are primarily attributable to the composition of the precursors, as detailed in Tables 1

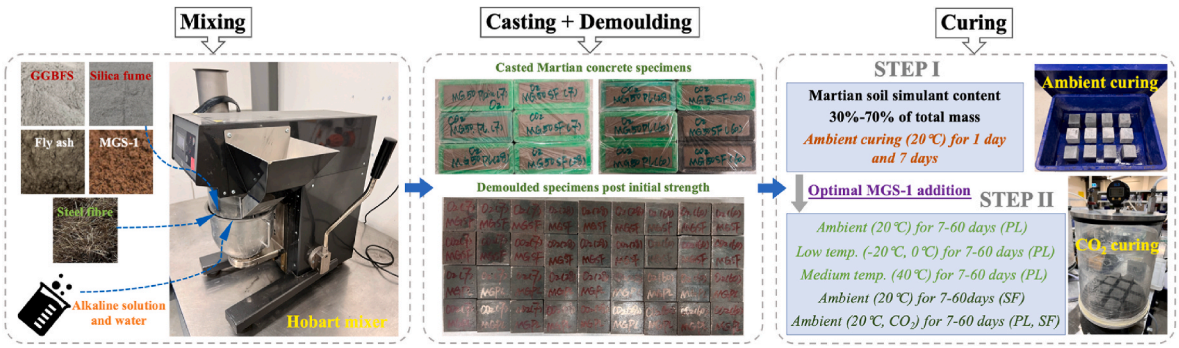

Fig. 3. Preparation and curing schematics of the HPMC specimens.

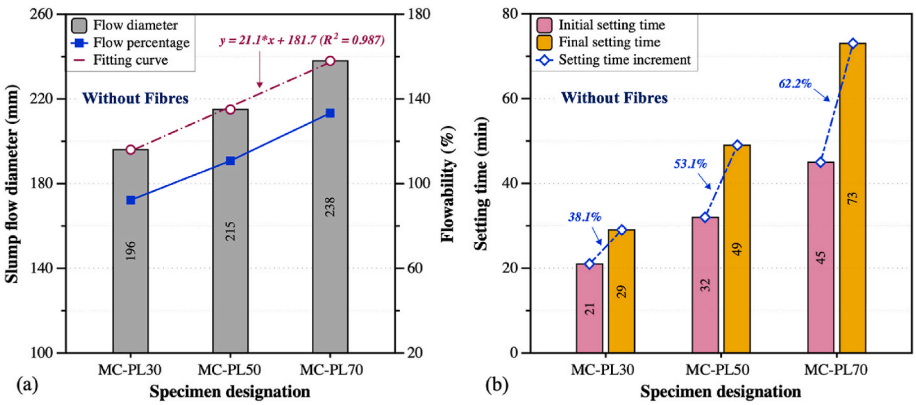

Fig. 4. Effect of MGS-1 content on (a) slump flowability and (b) setting time of HPMC.

and 2 At 30% MGS-1 content, GGBFS, rich in CaO, predominates, facilitating rapid formation of the calcium-associated gels during calcium ion reactions with water - an exothermic process that accelerates the geopolymer setting (Elyamany et al., 2018). In contrast, the higher MGS-1 additions (50% and 70%) result in fewer calcium ions and an increased presence of inert materials derived from the soil simulant, raising Na^{+} and OH^{-} levels. This adjustment slows aluminosilicate dissolution and reduces calcium leaching, delaying the geopolymerization processes relative to hydration reactions, and hence the setting times are notably extended (Karakoç et al., 2014).

3.1.2. Hardened mixture performance

Matrix density significantly influences the performance characteristics of concrete. Fig. 5(a) shows the density variations in hardened HPMC mixtures integrated with varying contents of soil simulant prior to mechanical testing. Notably, the density of the Martian concrete increased correspondingly as the mass percentage of MGS-1 in the mix was increased. Particularly, when the simulant addition was raised from 30% to 50%, the mean density experienced an evident increase of 6.2%, escalating from 2003.9 to 2128.9 kg/m^3. This enhancement is primarily attributable to the improved flowability of the fresh mixture, fostering enhanced compactness in the hardened state. Visibly, the diminished flowability and rapid setting in the MC-PL30 mix led to the formation of pronounced matrix defects in the fabricated concrete specimens, as demarcated by red circles in the figure, adversely affecting the compactness of the overall mixture. Furthermore, the intrinsically higher bulk density of MGS-1, as compared to the other solid materials as outlined in Table 1, also affected the hardened density of HPMC mixtures containing various simulant additions.

Fig. 5(b) demonstrates the effect of MGS-1 on the early compressive strength of Martian concrete. The depicted data are the averages from three cubic specimens cured for 1 and 7 days. A consistent increase in strength with curing time was observed across all mixes, reflecting substantial hydration and densification of binder materials. Strength gains of 69.5%, 68.8%, and 96.4% were recorded for MC-PL30, MC-PL50, and MC-PL70 mixes, respectively. The MC-PL50 mix achieved the highest compressive strengths, with values reaching 37.2 MPa at 1 day and 62.8 MPa at 7 days, exceeding the other mixes by 51.2% and 65.3% at 1 day, and 50.6% and 42.1% at 7 days, respectively. Typically, higher dosages of GGBFS benefited strength of geopolymer concrete by virtue of its rich content of reactive calcium, silicon, and aluminium oxides. These oxides, upon activation by an alkali activator, rapidly dissolved and interacted with alkali metal ions, forming a multidimensional and dense silico-aluminate framework (Xu et al., 2021). Besides, a high concentration of Ca^{2+} was crucial in synthesizing various hydration products, particularly the calcium silicate (C-S-H) gel, which acted as the nucleation sites facilitating the formation of stable and robust calcium/sodium aluminosilicate (C-A-S-H/(N)C-A-S-H) gels (Xie et al., 2019). However, an excessively high dosage of GGBFS (in mix MC-PL30) led to a relative deficiency of the alkali activator, surpassing its optimal reactive capacity, resulting in fewer soluble amorphous aluminosilicates and reduced total hydration products. Additionally, the poor flowability and matrix compactness of the MC-PL30 mixture likewise diminished the compressive strength of its specimens. When the MGS-1 addition was increased to 70% of the total mass (in mix MC-PL70), the content of CaO and active aluminosilicate components reduced, challenging the formation of a uniform, high-strength polymeric gel framework, consequently degrading the strength performance.

3.1.3. Microstructural performance

The SEM images of HPMC incorporating varying concentrations of MGS-1 are displayed in Fig. 6. The compressive performance of the

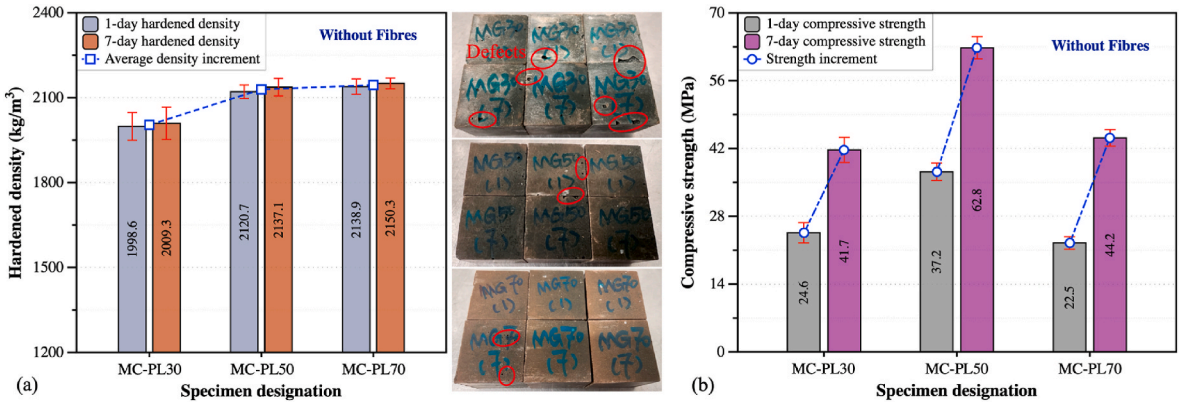

Fig. 5. (a) Hardened density and (b) compressive strength of HPMC with different contents of MGS-1.

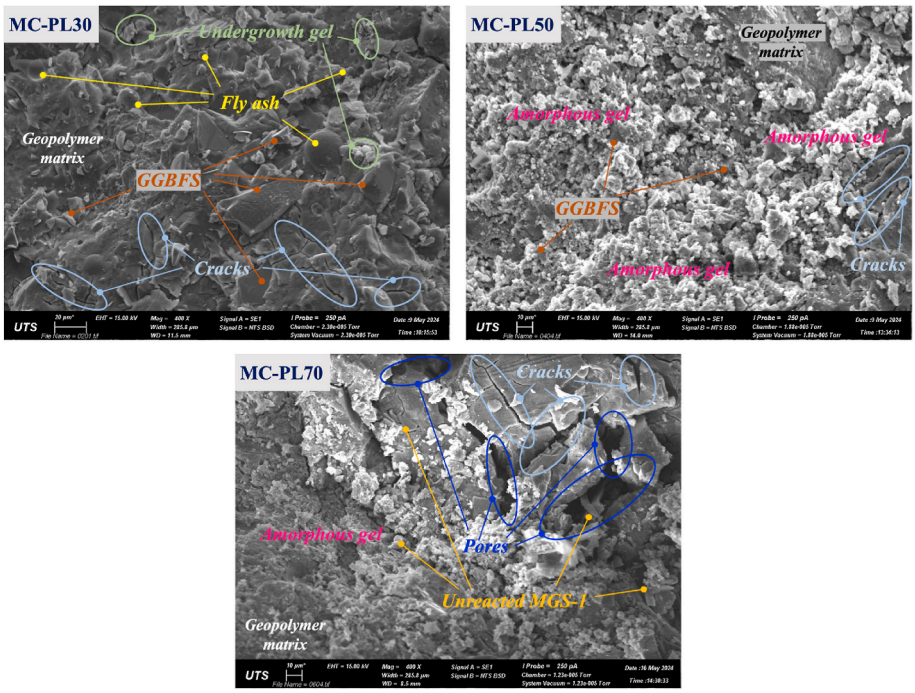

Fig. 6. SEM micrographs of HPMC mixtures incorporating 30%, 50%, and 70% of MGS-1.

formulated Martian concrete correlates with its microstructural characteristics. At a 30% simulant concentration by total mass, the micrograph reveals a compact microstructure without visible porosity despite the evident microcracks. In addition, the presence of substantial unreacted fly ash (smooth and spherical shape) and GGBFS (irregular and rough surface) particles, alongside immature amorphous gels, suggested that the alkali activation was insufficient for complete polymerization of the precursor materials. As the simulant content increased to 50%, a denser microstructure with fewer microcracks and a higher prevalence of amorphous gels (spherical stacks formed by granular particles (Zhou et al., 2021)) can be clearly observed. It is noteworthy that the formation of abundant gels during the geopolymerization process might partially mask or cover the unreacted or partially reacted GGBFS, fly ash, and silica fume. This effect resulted in less pronounced traces of these precursor particles within the binder phases, contributing to the observed differences in their morphologies. At this content, the alkali activation achieved the optimal effectiveness, as evidenced by the highest compressive strength of its hardened mixture. However, raising the simulant addition further to 70% deteriorated the microstructure, characterized by extensive internal defects, including pores and microcracks. The degradation is likely attributable to aluminosilicate precipitation, driven by the reduced availability of precursors and elevated alkali concentrations (Lee and Van Deventer, 2002). Moreover, a large quantity of unreacted MGS-1 particles (with specific morphologies illustrated in Fig. 1) embedded within the geopolymer matrix indicated an increased ratio of inert constituents of the simulant, which served as the aggregates and contributed to pore filling within the matrix.

Fig. 7 displays the EDS spectra of HPMC specimens containing various mass percentages of MGS-1, highlighting the identification of chemical components in the reaction products. The visualization of elemental distribution is enhanced by colour mapping the signal intensities of individual elements. Predominantly, the spectral revealed the presence of Si, Ca, Al, Na, Mg, and Fe across all specimens, corroborating the formation of a sodium/calcium aluminosilicate frame characteristic of geopolymer matrix. At a 30% mass inclusion of MGS-1, as depicted in Fig. 7(a), despite high signal intensities for Si, Al, and Ca, the reduced Na content hindered the adequate dissolution of the Si and Al in the precursor materials and subsequent polymerization reactions. Additionally, the elevated Ca levels impeded the effective formation of a stable calcium aluminate silicate hydrate (C-A-S-H) gel (Zhang et al., 2023a). The dispersed distribution of these elements within the colour mappings further supports this finding. As illustrated in Fig. 7(b) and (c), increasing the MGS-1 content to 50% and 70% led to a decline in atomic percentages of Si and Ca. However, the enhanced Na content more effectively facilitated the dissolution of Si and Al, promoting a more complete polymerization reaction. This enhancement allowed for a better interaction of Ca with the dissolved Si, Al, and other components in the alkaline environment, hydrating a dense and mechanically enhanced (N)C-A-S-H gel. The colour mappings indicate a more uniform elemental distribution, suggesting a denser microstructure filled with these gels. Nevertheless, it should be noted that in the mix MC-PL70, the signal intensity of Ca displayed a significant reduction, indicating a decrease in C-A-S-H gel content within the geopolymer matrix. Conversely, the content of sodium aluminate silicate hydrate (N-A-S-H) gel, structurally resembling zeolite, correspondingly increased. The colour mappings in this mix also reveal a more pronounced distribution of Fe and Mg elements, which can be attributed to the higher concentrations of iron and magnesium oxide in MGS-1 over other precursors. Research (Wu et al., 2024b; Hu et al., 2019; Zhang et al., 2024) suggested that while a suitable amount of iron silicate/magnesium silicate hydrate (F-S-H/M-S-H) could densify the microstructure of geopolymer concrete, an excessively high concentration of Fe and Mg may inhibit the growth of long polymeric chains and retard the geopolymerization process (M-S-H coating effect), increasing its porosity and consequently reducing the overall mechanical performance of the geopolymers.

Fig. 8 depicts the atomic ratios of key chemical elements crucial for the geopolymerization process in HPMC, derived from elemental analysis utilizing EDS data. Notably, the Si/Al ratio exhibited a decreasing trend as the inclusion of MGS-1 increased from 30% to 70%. This observation suggested enhanced dissolution of aluminium within the alkaline environment, facilitating the substitution of silicon by aluminium in the Si-O network, and promoting the formation of a more cohesive Si-Al tetrahedral framework (Krüger et al., 2023). The measured Si/Al ratios of 2.56 and 2.53 in the MC-PL50 and MC-PL70 mixtures, respectively, approached the optimal ratio (~2.50) identified by Xu et al. (2021) for the geopolymer-based UHPC (G-UHPC).

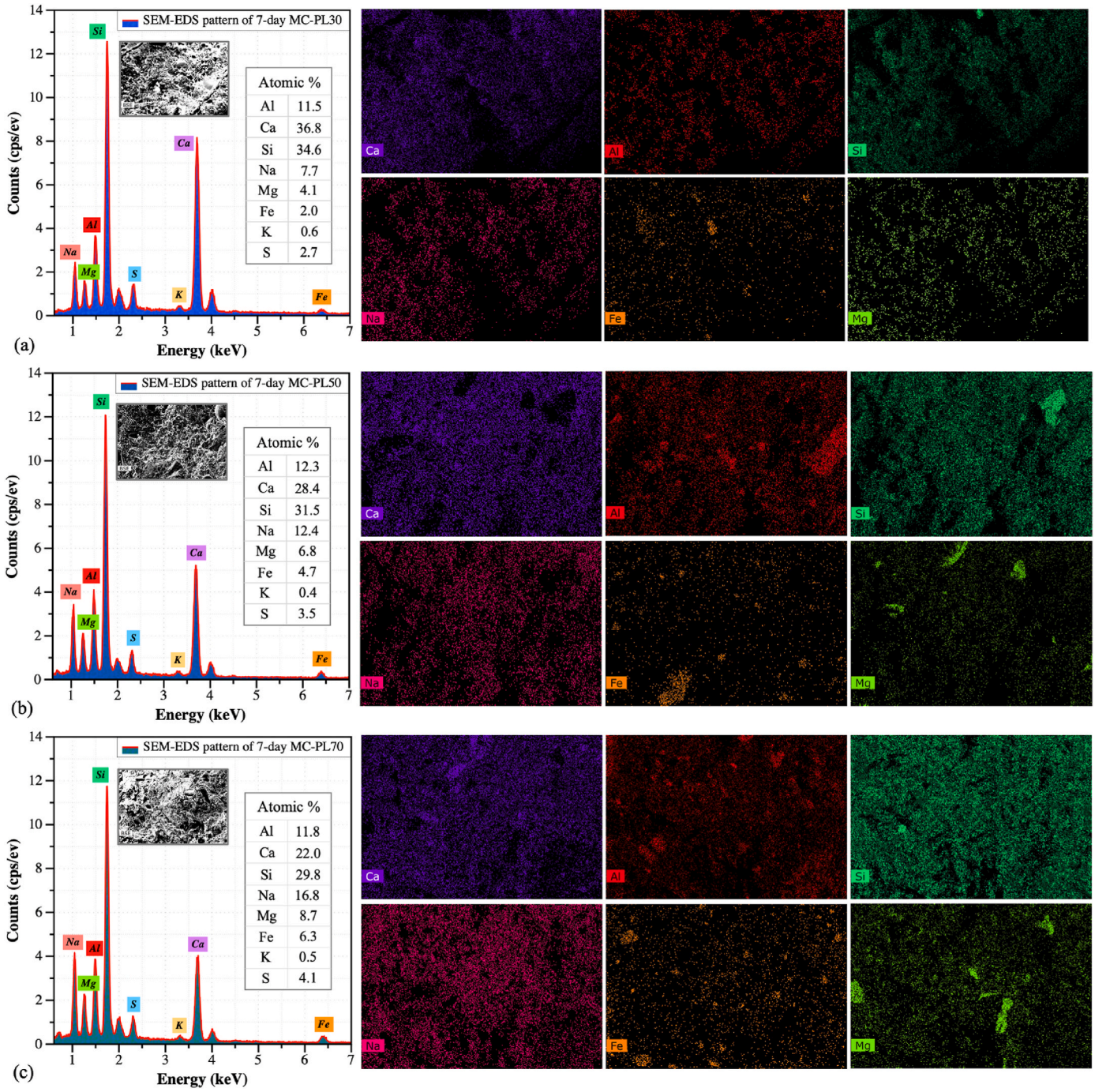

Fig. 7. SEM-EDS patterns of HPMC incorporating (a) 30%, (b) 50%, and (c) 70% of MGS-1.

Furthermore, the progressive reduction in the Si/Na ratios from 4.49 to 1.77 indicated an increase in sodium's role in the dissolution of the aluminosilicates. Nevertheless, the excessive sodium levels could precipitate premature efflorescence and obstruct the polycondensation in geopolymers by accelerating the coagulation of the dissolved species at an early reaction stage, potentially undermining the mechanical integrity (Nath and Kumar, 2019). In terms of Si/Ca ratios across three Martian concrete mixes, the inclusion of MGS-1 correlated with increased ratios, suggesting a decreased participation of Ca ions in the geopolymerization. This reduction in calcium involvement likely diminished the formation of C-A-S-H gels and the creation of Si-O-Ca bonds, which were typically more robust than those formed by sodium (Wang et al., 2024; Chitsaz and Tarighat, 2021).

XRD analysis is a highly effective method for identifying crystalline phases in the concrete matrix and assessing the degree of reactions (Trivedi et al., 2023). The phase compositions of HPMC synthesized with different MGS-1 dosages are shown in Fig. 9. Here, the principal mineralogical phases are identified following the standard Power Diffraction File (PDF) card. Notably, a broad peak ranging between 20° and 40° in diffraction angle highlights the formation of C-A-S-H and N-A-S-H gels within the HPMC matrix, consequent to the alkaline activation of aluminosilicate binders (Thakur and Ghosh, 2011). However, this broad feature may also encompass the amorphous contributions from unreacted precursor materials, which coexist with the reaction products in the alkali-activated system. The prominent mineralogical phase in the MC-PL30 mixture was identified as calcite at a 2θ of 29.4°.

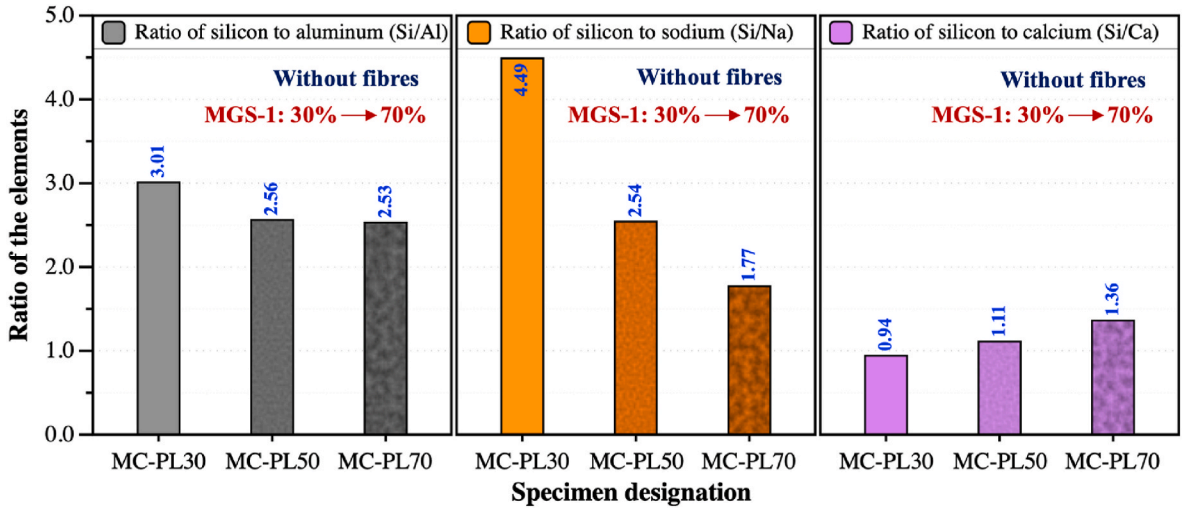

Fig. 8. Ratios of Si, Al, Na, and Ca detected by SEM-EDS on HPMC with various additions of MGS-1.

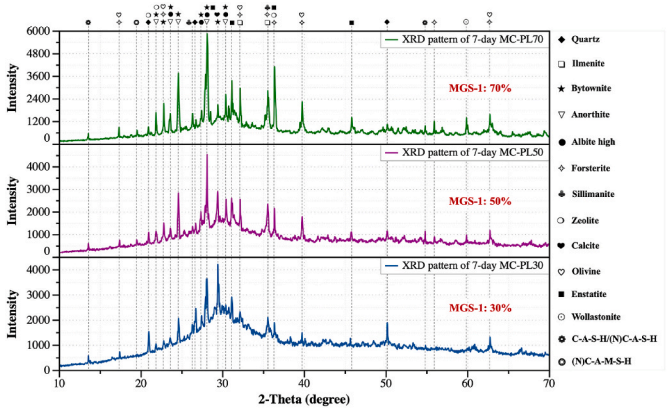

Fig. 9. XRD patterns of HPMC incorporating 30%–70% of MGS-1.

This peak more likely arises from two factors: (i) the presence of calcite impurities within GGBFS that persist when the material is insufficiently activated (Yu et al., 2023), and (ii) carbonation reactions involving the excessive amount of Ca^{2+} dissolved from GGBFS that reacts with OH^- and CO_2 in the open environment (Aziz et al., 2020). As the use of MGS-1 increased to 50% and 70%, the predominant phases identified were bytownite, albite high, and anorthite (major mineral constituents of MGS-1) at a 2θ of 28.1°, with a corresponding reduction in calcite intensity. This change suggests enhanced GGBFS participation in the geopolymerization reaction and reduced carbonation at lower Ca^{2+} concentrations. Furthermore, the proportion of inert components in MGS-1, serving as an aggregate filler, notably increased. It is particularly significant that albite might transition into combined C-A-S-H/(N) C-A-S-H gel structures in environments rich in Ca^{2+} ions (Xu et al., 2021), which further underscored the dual role of MGS-1 as both reactive precursors and aggregates. Moreover, the simultaneous reduction in quartz diffraction peaks at 2θ values of 20.8°, 26.6°, and 50.1° in the MC-PL50 and MC-PL70 mixtures correlates with a higher rate of amorphous gel formation and enhanced consumption of GGBFS in the geopolymerization reaction. Additionally, the intensities corresponding to forsterite and olivine peaks (at around 22.9°, 32.3°, 35.7°, and 36.5° for forsterite, and 17.3°, 22.8°, 32.3°, 39.6°, and 62.6° for olivine) were notably higher in MC-PL70, reflecting increased magnesium and iron content from the elevated MGS-1 concentrations.

3.1.4. Mass-strength efficiency

Given the prohibitive cost of transporting raw materials from Earth to Mars, Martian concrete should optimize ISRU while maintaining requisite strength properties. In this context, the concept of "mass-strength efficiency" (Zhou et al., 2021) was introduced to evaluate the potential for mass savings while achieving specified strength levels in HPMC containing various contents of MGS-1. Previous studies, such as those by Hadnott et al. (2017), have demonstrated the feasibility of producing an alkaline solution in-situ using alkali metals found on Mars. Thus, the efficiency calculations were performed comparing scenarios where the alkali activator sourced from Earth versus Mars. The respective efficiencies are detailed in Equations (1) and (2):

$$\eta_{msE} = \left[\left(m_{GGBFS} + m_{silica\ fume} + m_{fly\ ash} + m_{activator}\right) \times 100 \,/\, \left(m_{MGS-1} + m_{water}\right) \times f_c\right]^{-1} \quad (1)$$

$$\eta_{msM} = \left[\left(m_{GGBFS} + m_{silica\ fume} + m_{fly\ ash}\right) \times 100 \,/\, \left(m_{MGS\text{-}1} + m_{activator} + m_{water}\right) \times f_c\right]^{-1} \quad (2)$$

where η_{msE} and η_{msM} represent the mass-strength efficiency of HPMC with alkali activator sourced from Earth and Mars, respectively (MPa), m_x denotes the mass of various components, and f_c is the compressive strength of HPMC (MPa). Fig. 10 illustrates the variations in mass-strength efficiency of HPMC following curing periods of 1 and 7 days. Observations indicate that both scenarios exhibit enhanced compression efficiency with curing time and MGS-1 content, particularly in mixes MC-PL50 and MC-PL70, where efficiency markedly improved from day 1 to day 7. Notably, producing the alkali activator on-site on Mars enabled a 92.7%–112.9% increase in compression efficiency. For instance, in the MC-PL70 mixture, the significant increase in 7-day efficiency from 0.650 MPa to 1.382 MPa suggested that for each unit mass of Mars-sourced ISRU converted into 1.0 MPa of compressive strength, the in-situ activator could potentially reduce costs by 81.5%. Importantly, the efficiency showed a more marked increase from 30% to

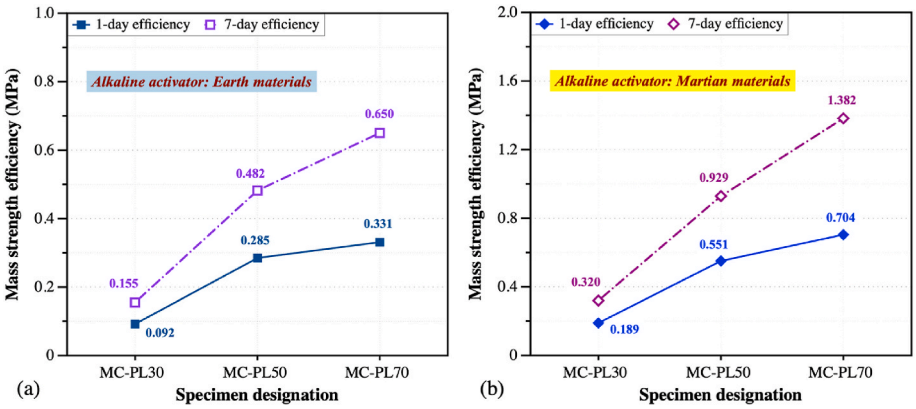

Fig. 10. Mass-strength efficiency in compression with alkali activator sourced from (a) Earth and (b) Mars.

50% MGS-1 content, especially after 1 day of curing. Following comprehensive evaluation of the strength and microstructural performance as reported above, the MC-PL50 mix has been identified as the optimal choice for Martian construction, offering the highest early strength and rapid efficiency increase. Further study will explore the effect of diverse temperature and atmospheric conditions on this optimal Martian concrete mixture.

3.2. Effect of diverse temperatures

3.2.1. Hardened mixture performance

The optimized Martian concrete mixtures MC-PL50 were cast and subjected to initial consolidation for 24 h. Subsequently, the specimens were exposed to a range of curing temperatures of 40 °C, 20 °C, 0 °C, and −20 °C up to the testing period. As depicted in Fig. 11(a), a clear gradation in colour lightning of the specimens was observed with increasing curing temperatures. Notably, the colour variation intensified as the curing period extended from 7 to 60 days. This change may stem from the accelerated migration of alkali ions at 40 °C, resulting in the formation of visible white carbonate deposits on the concrete surface. Conversely, at sub-zero temperatures (0 °C and −20 °C), the rate of geopolymerization reactions was reduced, inhibiting the conversion of dark-coloured materials such as fly ash, silica fume, and MGS-1. This slowdown also curtailed the migration of alkaline ions and carbonation reactions, preserving the darker surface colouration. It is noteworthy that an evident development of microcracks was observed in specimens cured at 40 °C, which became increasingly visible with prolonged curing. This phenomenon is mainly attributed to the accelerated evaporation of water at elevated temperatures, leading to disparate rates of drying shrinkage between the surface layer and the internal matrix.

Fig. 11(b) illustrates the density variations in hardened HPMC mixtures subjected to different curing temperatures prior to mechanical testing. The data indicates that all mixtures, except MC50PL40C, maintained similar hardening densities across varying ages. However, at 40 °C, there was an evident decrease in specimen density from 2128.8 to 1973.2 kg/m^3 (reduced by 7.3%) over time, which was attributed to the progressive water loss as well as the reduction in matrix compactness exacerbated by cracking phenomena.

Fig. 11(c) presents the effects of curing temperature on the compressive strength of HPMC over a period of 60 days. The data clearly indicates that the specimens cured at 40 °C exhibited the highest initial compressive strength, yielding 71.8 MPa, which substantially exceeded the strength observed in specimens cured at other three temperatures (62.8, 47.4, and 50.3 MPa). This enhancement can be ascribed to the

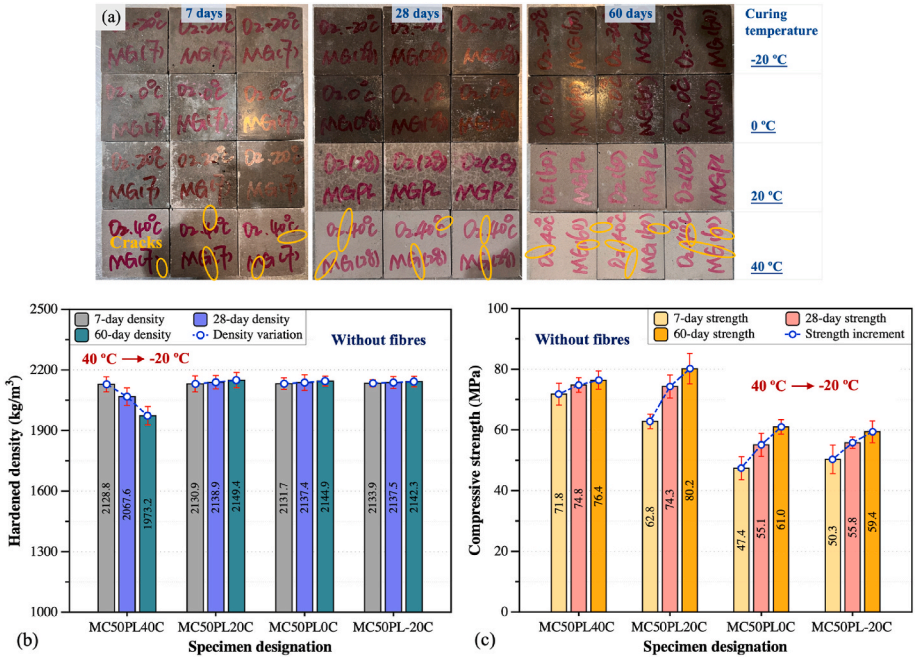

Fig. 11. Effect of curing temperature on (a) specimen appearance, (b) hardened density, and (c) compressive strength of HPMC.

accelerated geopolymerization process at elevated temperatures, which facilitated more rapid polymerization and crosslinking of the aluminosilicate tetrahedron, leading to extensive gel phase formation (Nurruddin et al., 2018). However, the specimens cured at 20 °C displayed a remarkable increase in strength development, exhibiting an 18.3% increase at 28 days and achieving the highest 60-day strength of 80.2 MPa. This strength gain outpaced increments of 5.0%, 31.5%, and 35.0% observed in the other groups, respectively. The reduced rate of strength development in specimens labelled as MC50PL40C can be attributed to decreased hardening density associated with continual water loss, which significantly slowed the rate of geopolymerization in later stages, while shrinkage cracking further impaired the load-bearing capacity of the geopolymers. For specimens cured at 0 °C and −20 °C, the observed lower strengths across all testing ages could primarily be due to the increased viscosity of the alkali activation solution in cold conditions or the markedly reduced dissolution rate of the aluminosilicate compounds and gel formation, a result of partial freezing (Zhang et al., 2023b). It is noteworthy that the 7-day compressive strength of the MC50PL-20C specimen was slightly higher than that of the MC50PL0C specimen, although at 60 days, the latter exhibited superior performance. This may be linked to the state of water within the geopolymer matrix. As noted by Huo et al. (2022), the freezing points of different states of water within the concrete matrix varied significantly: free water at about 0 °C, capillary water at −10 to −30 °C, gel water at −43 °C, and absorbed water at −60 to −130 °C. Therefore, at −20 °C, a higher proportion of water was likely to freeze, initially filling the micropores within the geopolymer and forming a denser matrix. Nevertheless, over longer periods under lower-temperature curing, the greater proportion of frozen water impeded the geopolymerization reaction rate, delaying or even preventing complete curing and thus slowing strength development in HPMC.

The modulus of elasticity (MOE) serves as a critical metric for assessing the capacity of concrete to withstand elastic deformation under applied stress. Fig. 12(a) illustrates the variations in MOE for HPMC after 28 and 60 days under different curing temperature conditions. These values represent the mean of three cubic specimens derived from compression tests, where the stress increment was divided by the corresponding axial strain variation. These measurements were facilitated by the DIC system, which accurately recorded the real-time strain data on the surface of each specimen. Results revealed that the MOE notably enhanced with an extended curing period. Furthermore, the trend in MOE variations mirrored the changes observed in compressive strength under analogous conditions. This correlation likely stems from the MOE being primarily derived from the elastic portion of the compressive stress-strain relationship in concrete, wherein the MOE generally fluctuates in response to variations in compressive strength. It is particularly noteworthy that the mixtures cured at 20 °C exhibited the highest MOE values at both tested ages: 29.4 GPa after 28 days and 30.3 GPa after 60 days. Conversely, the mixtures cured at sub-zero temperatures (0 °C and −20 °C) displayed the lowest MOE values, with reductions of 14.5% and 13.9% at 60 days in comparison with the MC50PL20C mixture, respectively. Moreover, when examining the compressive strength, mixtures cured at these sub-zero temperatures demonstrated reductions of 23.9% and 25.9% under the same conditions (as illustrated in Fig. 11(c)). This discrepancy suggests that the MOE may be less sensitive to the low temperatures as compared to compressive strength of geopolymer-based Martian concrete. Fig. 12(b) delineates the correlation between the compressive strength and the MOE of HPMC across different curing temperatures and periods. This scatter plot indicates a robust power relationship between the strength and MOE, as confirmed by the derived regression model $MOE = 3172.1 \cdot f_c^{0.5} + 1453.1$ with a coefficient of determination of 0.941, for compressive strengths ranging from 55 MPa to 80 MPa.

3.2.2. Microstructural performance

Fig. 13 shows representative SEM images of HPMC samples containing fly ash particles, examined under various curing temperatures. In MC50PL-20C mix, cured at −20 °C, the spherical morphology of the fly ash particle was largely maintained, with minimal adhesion of amorphous gel on its surface. This observation suggests that the geopolymerization reaction is substantially hindered at such low temperatures, with limited particle dissolution and subsequent geopolymer formation. At a slightly higher curing temperature of 0 °C (MC50PL0C mix), the image reveals an increased envelopment of the fly ash particles by more amorphous gel, blurring their distinct outlines and indicating a partial advancement in the reaction process. Progressing to 20 °C (MC50PL20C mix), it becomes difficult to identify the individual fly ash particles within the SEM micrographs, pointing to a more complete geopolymerization reaction and the formation of a dense, uniform geopolymer matrix. However, at 40 °C (MC50PL40C mix), despite the formation of a denser matrix, the rapid moisture evaporation and accelerated reaction rate associated with this elevated temperature prevented some fly ash from fully reacting, as evidenced by their visibility within the matrix. This incomplete reaction adversely influences the long-term strength development of the material. The depicted micrographs provide a detailed microstructural explanation for the observed variations in mechanical properties of HPMC across a curing temperature range from −20 °C to 40 °C, offering crucial insights for the design and optimization of concrete suitable for Martian environments.

3.3. Effect of atmospheric environment

3.3.1. Hardened mixture performance

To evaluate the impact of different atmospheric conditions on the performance of HPMC with and without steel fibre reinforcement, two variants named MCSF and MCPL were synthesized based on the optimized MC-PL50 mixture. Initially, these specimens underwent the consolidation for 24 h and were subsequently subjected to either ambient or CO_2-rich environments for curing until testing ages. As illustrated in Fig. 14(a), the specimens exposed to the carbonated curing

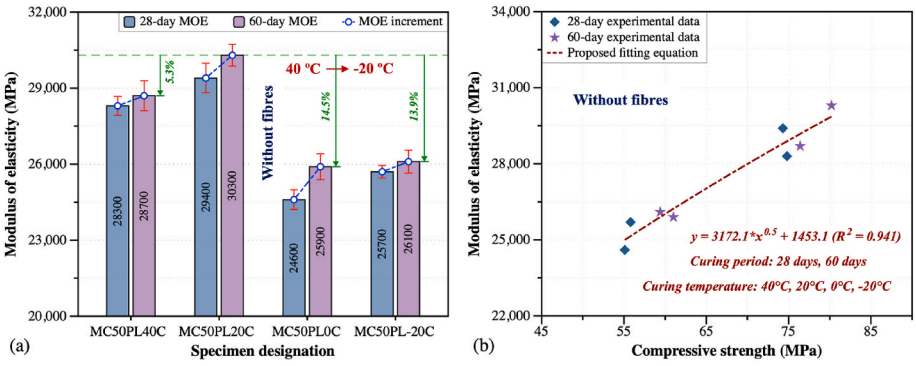

Fig. 12. (a) Static MOE and (b) its correlation with compressive strength of HPMC under various curing temperature conditions.

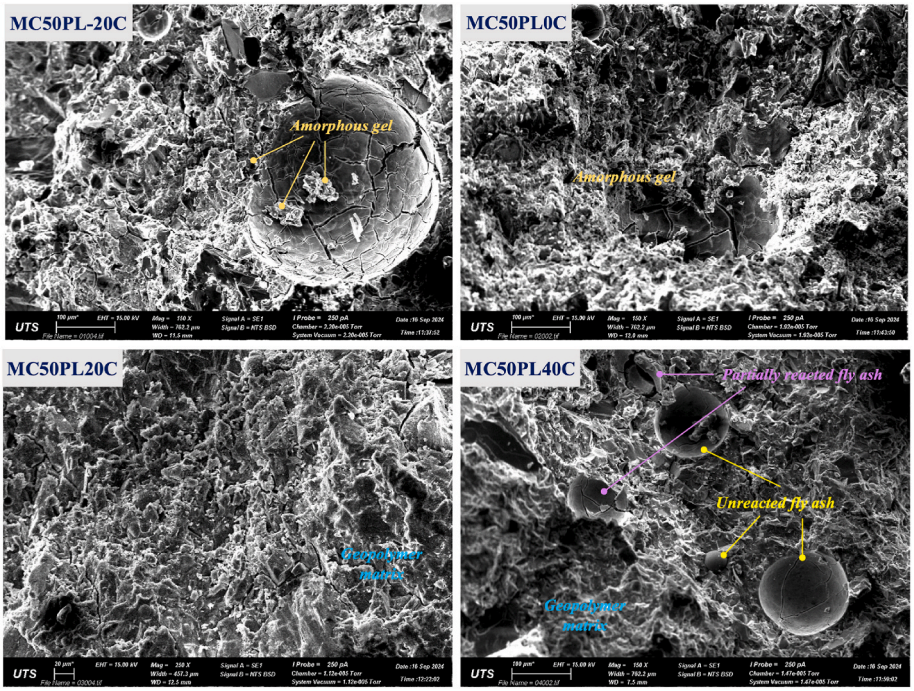

Fig. 13. Typical SEM images of HPMC focusing on fly ash particles with various curing temperatures.

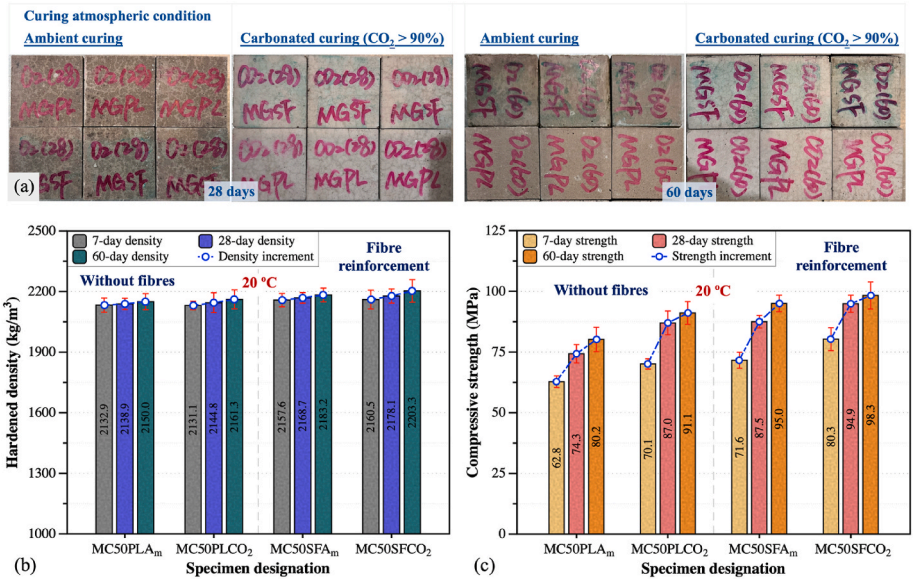

Fig. 14. Effect of curing atmospheric condition on (a) specimen appearance, (b) hardened density, and (c) compressive strength of HPMC with and without fibre reinforcement.

displayed a notable increase in brightness, a manifestation of the carbonation process wherein the calcium phases in the binder reacted with CO_2 to form calcium carbonate ($CaCO_3$) (Sai Trivedi et al., 2023). The brightening effect intensified as the curing extended from 28 to 60 days, indicating progressive and more extensive carbonation. Conversely, the specimens cured in ambient conditions exhibited consistent colouration throughout the period, suggesting a stable yet less chemically interactive environment. Notably, these ambient-conditioned samples showed minor surface microcracking, while those in the CO_2-rich atmosphere maintained a smooth surface. This implies that the carbonate layer formed during carbonation serves a protective role, potentially shielding the Martian concrete by reducing moisture loss and impeding pollutant penetration.

Fig. 14(b) showcases a comparison of the hardening density of HPMC with and without steel fibre reinforcement at three curing periods under two atmospheric conditions. The inclusion of steel fibres consistently resulted in a denser matrix across all the measured intervals and environmental settings. Notably, the use of fibres elevated the average density from 2140.6 to 2169.8 kg/m^3 in specimens cured under ambient conditions. This improvement was largely attributable to the fibres enhancing the microstructure by reducing porosity and increasing compactness within the matrix. The superior inherent density of steel fibres over other constituent materials also contributed significantly to this density enhancement. Additionally, the atmospheric condition further affected the curing dynamics of HPMC. Specimens exposed to a CO_2-rich atmosphere showed an increase in density as compared to

those cured in ambient air. For instance, after 60 days, the density of MCPL mixtures rose from 2150 to 2161.3 kg/m^3, and from 2183.2 to 2203.3 kg/m^3 in MCSF mixtures. This effect was likely due to the carbonation reaction within the geopolymer matrix, where CO_2 exposure led to carbonate crystallization, filling micro-voids and thereby augmenting matrix densification (Bang et al., 2023).

Fig. 14(c) shows the compressive strength development of HPMC under two atmospheric conditions over a period of up to 60 days. In the ambient environment, MCPL specimens consistently exhibited lower strength values at all measured intervals as compared to MCSF counterparts. This discrepancy underscores the crucial role of steel fibres in enhancing the mechanical properties of HPMC through improved crack resistance and more effective load distribution within the geopolymer matrix. As an illustration, at 28 and 60 days, the compressive strengths of MCSF specimens reached 87.5 and 95.0 MPa, respectively, marking increases of 17.8% and 18.5% over the MCPL cases. When subjected to carbonation curing, both Martian concrete variants demonstrated enhanced compressive strength relative to those cured in ambient air, with the increase being more pronounced in the geopolymers without fibres. Specifically, MCPL specimens displayed increases in strength of 17.1% and 13.6% at 28 and 60 days, respectively, while MCSF counterparts showed increases of 8.5% and 3.5% for the same ages. This trend can be attributed to the higher contents of calcium and silicon within the matrix (refer to Fig. 7(b)), which, under the influence of CO_2 exposure, facilitated the precipitation of $CaCO_3$ polymorphs within void spaces adjacent to the calcium-rich phases, as well as potentially amorphous SiO_2 gels resulting from decalcification processes (Lamaa et al., 2023). Moreover, the decalcification of C-A-S-H gels, where CO_2 penetrated the concrete matrix and reacted with calcium ions in the gel structure, further contributes to the formation of $CaCO_3$ and silica-rich phases (Bernal et al., 2013). These reactions were beneficial to a more cohesive and denser matrix, significantly improving the integrity of HPMC. Nevertheless, extended exposure to high concentrations of CO_2 may induce micro-defects or initial cracking within the matrix, and compromised the alkaline environments essential for gel formation of the geopolymers (Bernal et al., 2011). The reduction of alkalinity could accelerate the corrosion of the embedded steel fibres, especially at locations of cracks or voids, thus weakening their toughening effect within the fibre-reinforced Martian concrete.

Fig. 15(a) illustrates the typical compressive stress-strain responses of HPMC (MCPL and MCSF specimens) under two atmospheric conditions after 60 days of curing. The graphical representation was generated using real-time data, which was obtained from the compressive loads measured by a testing apparatus and the axial strain changes detected by a DIC system. The data clearly shows that the inclusion of steel fibres signally enhanced both the compression capacity and the deformability of the concrete matrix up to the point of softening. Notably, in ambient environments, the peak stress for the HPMC increased from 78.8 MPa at a strain of 0.00301 (MCPL mix) to 95.6 MPa at a strain of 0.00334 (MCSF mix). Additionally, the inclusion of fibres notably reduced the brittleness of the concrete matrix post-peak, as evidenced by a less pronounced drop in stress and a broader area under the curves at the same strain levels. However, under prolonged exposure to a CO_2 environment, the beneficial effects of fibre incorporation were markedly diminished. Furthermore, carbonation curing positively affected the compression capacity and peak strain of HPMC without fibre reinforcement, as observed in the comparative analysis of stress-strain characteristics.

Fig. 15(b) displays the failure modes of HPMC samples subjected to ambient and carbonation curing conditions. The visual representation clearly highlights the differential effects of fibre reinforcement and environmental conditions on the integrity of the specimens. Under both curing conditions, the MCPL specimens exhibited a brittle failure mode characterized by the conical fracturing. In contrast, the fibre-reinforced MCSF specimens demonstrated enhanced matrix integrity with reduced surface spalling, indicating significantly improved ductility and toughness. However, it is important to note that specimens carbon-cured for 60 days exhibited more pronounced structural damage as compared to those cured for 28 days, suggesting a considerable weakening in the fibres' effectiveness at aiding the geopolymers in resisting crack formation and propagation.

Fig. 16(a) delineates the variations in the static MOE of HPMC subjected to both atmospheric curing conditions at 28 and 60 days. Derived from the slope of the linear-elastic region on the stress-strain curves, as illustrated in Fig. 15(a), the MOE results indicated a discernible increase with extended curing periods. Notably, the addition of steel fibres prominently enhanced the MOE, particularly in specimens cured in ambient air, where the 60-day MOE observed a 7.3% increase from 30.3 to 32.5 GPa. In carbon-cured specimens, the increment was 4.4%, from 31.7 to 33.1 GPa. When combining fibre reinforcement and carbonation curing, the increments in 28- and 60-day MOE reached 11.9% and 9.2%, respectively, suggesting that both methods effectively improved the matrix microstructure and stiffness. However, the efficacy of fibre reinforcement diminished with prolonged exposure in high CO_2 environments.

The regression equation $MOE = 3172.1 \cdot f_c^{0.5} + 1453.1$, derived from the analysis of various curing temperatures in Section 3.2.1., is employed to investigate the interdependency between compressive strength and MOE for the HPMC under varied atmospheric conditions, as illustrated in Fig. 16(b). By extending the initial compressive strength range from 55–80 MPa to 55–100 MPa, the updated regression model exhibited improved predictability of MOE across different compressive strength behaviours under ambient and carbonation conditions (highlighted by the green cubic points). This adjustment yielded an enhanced

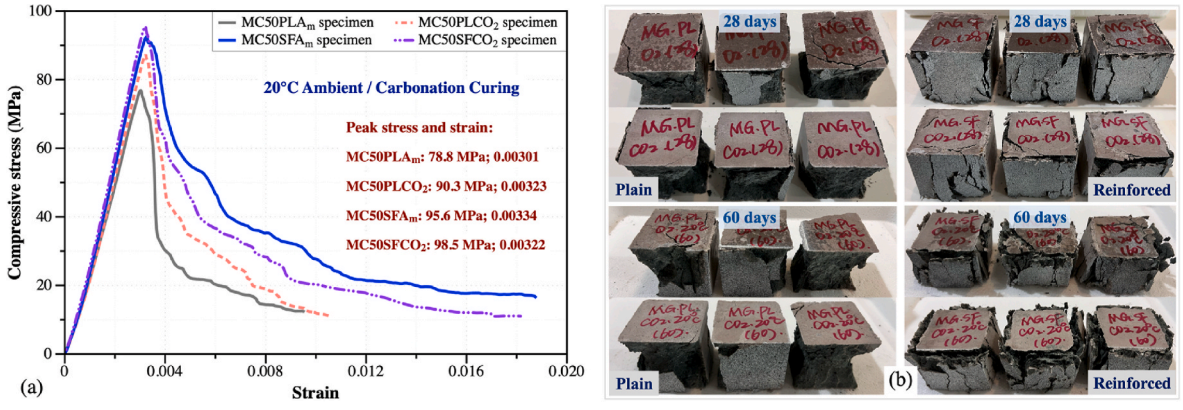

Fig. 15. (a) Typical 60-day compressive stress-strain curves and (b) failure patterns of HPMC with and without fibre reinforcement after ambient and carbonation curing.

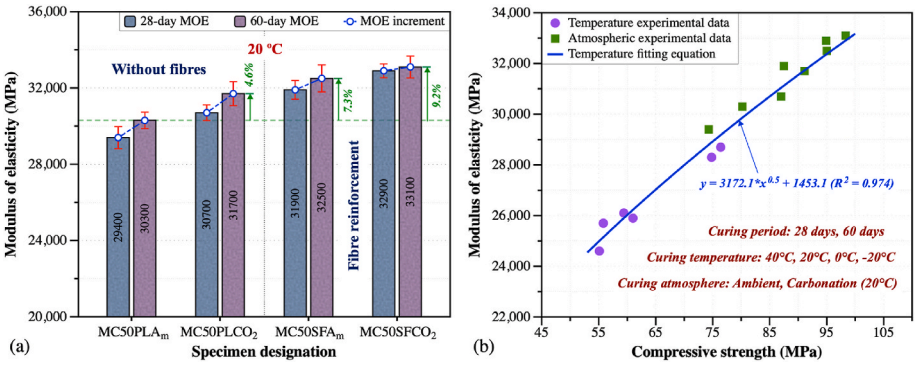

Fig. 16. (a) Static MOE and (b) its correlation with compressive strength of HPMC cured with various atmospheric conditions.

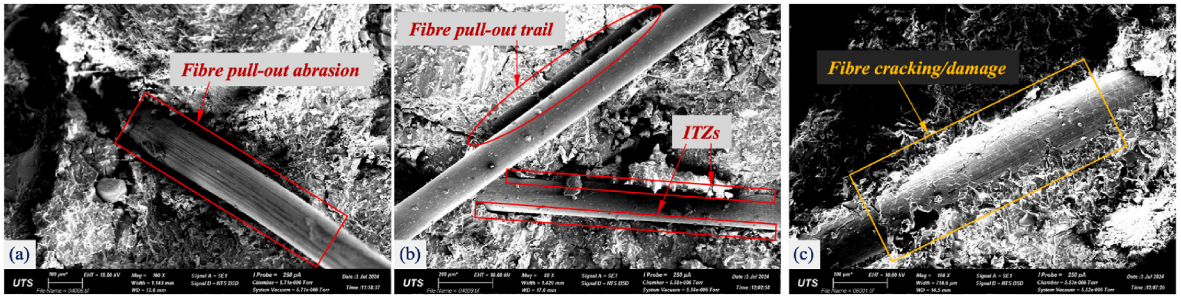

Fig. 17. SEM micrographs of HPMC matrix with steel fibre reinforcement under (a–b) ambient and (c) carbonation curing conditions.

R^2 value of 0.974, up from 0.941, underscoring the model's robust predictive reliability across diverse temperature and atmospheric curing environments.

3.3.2. *Microstructural performance*

Fig. 17 presents the typical SEM images of HPMC reinforced with steel fibres in varied atmospheric environments. Fig. 17(a) and (b) depict the matrix under ambient curing conditions, where steel fibres were clearly embedded within the geopolymer matrix. Upon loading, the fibres were observed to gradually detach from the matrix, demonstrating notable fibre surface abrasion and the formation of pull-out trails. These phenomena are indicative of the mechanical interlocking provided by the steel fibres, which is important for inhibiting the rapid propagation of macro-cracks and bolstering the structural integrity of HPMC matrix. This interaction underscores the effective adhesion quality of the matrix and the critical function of mechanical anchorage in enhancing energy absorption of the concrete. Fig. 17(c) examines the matrix under carbonation curing conditions, revealing distinct microstructural alterations. The carbonation process, characterized by the reaction of CO_2 with the geopolymer components, results in carbonate crystallization in the geopolymer matrix. This reaction typically engenders a denser microstructure as carbonate precipitates occlude micro-voids, evident from the more compact interfacial transition zones (ITZs) between the steel fibre and the matrix, in contrast to those observed in Fig. 17(b). It is crucial to note, however, that the steel fibre exhibited pronounced matrix cracking and damage. This damage is mainly ascribed to the prolonged exposure to elevated CO_2 concentrations, which disrupts the alkaline environment, therefore precipitating the corrosion of the steel fibres.

4. Conclusions

In this research, a high-performance Martian concrete (HPMC) was synthesized utilizing a synthetic Martian regolith simulant, MGS-1. The prepared Martian geopolymers were examined with varying amounts of simulant content, and the impact of curing regimes, comprising various temperature and atmospheric conditions over different curing periods, was systematically investigated. The findings from this research are summarized as follows.

1) HPMC shows extended setting times and improved matrix compactness with increased MGS-1 contents. A mixture containing 50% MGS-1 demonstrates the highest compressive strength of 62.8 MPa at 7 days, compared with 44.2 and 41.7 MPa for 70% and 30% MGS-1 contents, respectively.
2) The mixture with 50% MGS-1 shows ideal Si/Al, Si/Na, and Si/Ca ratios, promoting efficient geopolymerization and prolific formation of C-S-H, C-A-S-H, and N-A-S-H gel. The dual role of MGS-1 as both a precursor and aggregate is highlighted through XRD analysis.
3) The mass-strength efficiency of HPMC improves with longer curing and higher MGS-1 content. Overall, the mixture with 50% MGS-1 provides the best balance of early strength and efficiency, making it the optimal choice for Martian construction.
4) HPMC cured at 0 °C and −20 °C consistently achieves the lowest compressive strengths due to the reduced dissolution rate of aluminosilicate compounds and limited gel formation. In contrast, curing at 40 °C and 20 °C, respectively, shows superior early and long-term strength. The higher temperature accelerates moisture loss, slows the geopolymerization rate, and induces shrinkage cracking in the matrix.
5) Carbonation curing and steel fibre inclusion both markedly improves the matrix compactness and compressive behaviour of HPMC, with a peak strength of 98.3 MPa observed in the fibre-reinforced specimen after 60 days of carbonation curing. However, the prolonged CO_2 exposure reduces the fibres' toughening effect, as indicated by visible matrix cracking and damage to the steel fibres.

5. Limitations

Despite the encouraging results presented in this study, several

limitations warrant consideration for future research and practical implementation, particularly in the context of off-Earth construction:

1) This study employed GGBFS, silica fume, and fly ash, which are not realistically available on Mars. Although these precursors served as performance benchmarks, future research will focus on developing and testing high/ultra-high performance Martian geopolymers, relying solely on Martian regolith or locally synthesized materials.
2) A relatively high AAS dosage was adopted to ensure rapid and complete geopolymerization. While this dosage improves mechanical performance, it raises concerns regarding logistical challenges of transporting or synthesizing large quantities of activators on Mars. Lowering the activator dosage through optimizing mix design or developing ISRU-derived activators remains a priority for sustainable off-Earth construction.
3) While steel fibres notably enhance the mechanical properties of HPMC, the mass and energy costs of transporting steel from Earth are prohibitive for large-scale use on Mars. Moreover, the capricious conditions on Mars may pose further challenges to steel durability. Alternative materials, such as basalt fibres derived from Martian minerals, could offer a more practical route for reinforcement under off-Earth conditions.
4) While the study examines the behaviour of Martian concrete between −20 °C and 40 °C, this temperature range does not fully capture the actual −63 °C Martian average (Reches, 2019). Future work will explore testing at lower temperatures to gain a more accurate evaluation of how Martian concrete performs in true Martian-like environments.

Addressing these limitations is crucial for advancing the concept of in-situ Martian constructions. Building on these findings, a more robust experimental framework emphasizing lower operational temperatures, increased use of Martian soil, and minimized reliance on external raw materials will significantly enhance the feasibility of developing sustainable, self-sufficient construction methods for future extra-terrestrial habitats.

CRediT authorship contribution statement

Ruizhe Shao: Writing – original draft, Methodology, Investigation, Conceptualization. **Chengqing Wu:** Writing – review & editing, Visualization, Supervision, Resources, Methodology, Conceptualization. **Jun Li:** Writing – review & editing, Methodology, Conceptualization.

Declaration of competing interest

The authors declare that they have no known competing financial interests or personal relationships that could have appeared to influence the work reported in this paper.

Acknowledgement

The study presented herein is supported by ARC Discovery Grant DP210101100. Thanks are due to UTS TechLab staff Benjamin Smith and PhD student Zizheng Yu for the assistance with experiments.

Data availability

Data will be made available on request.

References

Akono, A.-T., 2023. Influence of martian soil simulant on microstructural heterogeneity and mechanical response of Martian concretes. Mech. Res. Commun. 127, 104013.
ASTM C109/C109M, 2013. Standard Test Method for Compressive Strength of Hydraulic Cement Mortars. American Society for Testing and Materials, Philadelphia.
ASTM C1437, 2013. Standard Test Method for Flow of Hydraulic Cement Mortar. American Society for Testing and Materials, Philadelphia.
ASTM C191, 2013. Standard Test Methods for Time of Setting of Hydraulic Cement by Vicat Needle. American Society for Testing and Materials, Philadelphia.
Aziz, I.H., Abdullah, M.M.A.B., Salleh, M.M., Azimi, E.A., Chaiprapa, J., Sandu, A.V., 2020. Strength development of solely ground granulated blast furnace slag geopolymers. Constr. Build. Mater. 250, 118720.
Bang, J., Choi, J., Hong, W.-T., Jung, J., Kim, G.M., Yang, B., 2023. Influences of binder composition and carbonation curing condition on the compressive strength of alkali-activated cementitious materials: a review. J. CO2 Util. 74, 102551.
Bernal, S.A., de Gutiérrez, R.M., Pedraza, A.L., Provis, J.L., Rodriguez, E.D., Delvasto, S., 2011. Effect of binder content on the performance of alkali-activated slag concretes. Cement Concr. Res. 41 (1), 1–8.
Bernal, S.A., Provis, J.L., Walkley, B., San Nicolas, R., Gehman, J.D., Brice, D.G., Kilcullen, A.R., Duxson, P., van Deventer, J.S., 2013. Gel nanostructure in alkali-activated binders based on slag and fly ash, and effects of accelerated carbonation. Cement Concr. Res. 53, 127–144.
Cannon, K.M., Britt, D.T., Smith, T.M., Fritsche, R.F., Batcheldor, D., 2019. Mars global simulant MGS-1: a Rocknest-based open standard for basaltic martian regolith simulants. Icarus 317, 470–478.
Chitsaz, S., Tarighat, A., 2021. Estimation of the modulus of elasticity of NASH and slag-based geopolymer structures containing calcium and magnesium ions as impurities using molecular dynamics simulations. Ceram. Int. 47 (5), 6424–6433.
Elyamany, H.E., Abd Elmoaty, M., Elshaboury, A.M., 2018. Setting time and 7-day strength of geopolymer mortar with various binders. Constr. Build. Mater. 187, 974–983.
Fackrell, L.E., Schroeder, P.A., Thompson, A., Stockstill-Cahill, K., Hibbitts, C.A., 2021. Development of Martian regolith and bedrock simulants: potential and limitations of Martian regolith as an in-situ resource. Icarus 354, 114055.
Gonçalves, T., Silva, R., De Brito, J., Fernández, J., Esquinas, A., 2020. Mechanical and durability performance of mortars with fine recycled concrete aggregates and reactive magnesium oxide as partial cement replacement. Cement Concr. Compos. 105, 103420.
González-García, D., Téllez-Jurado, L., Jiménez-Álvarez, F., Balmori-Ramírez, H., 2017. Structural study of geopolymers obtained from alkali-activated natural pozzolan feldspars. Ceram. Int. 43 (2), 2606–2613.
Hadnott, B.A., Ehlmann, B.L., Jolliff, B.L., 2017. Mineralogy and chemistry of San Carlos high-alkali basalts: analyses of alteration with application for Mars exploration. Am. Mineral. 102 (2), 284–301.
Hu, Y., Liang, S., Yang, J., Chen, Y., Ye, N., Ke, Y., Tao, S., Xiao, K., Hu, J., Hou, H., Fan, W., Zhu, S., Zhang, Y., Xiao, B., 2019. Role of Fe species in geopolymer synthesized from alkali-thermal pretreated Fe-rich Bayer red mud. Constr. Build. Mater. 200, 398–407.
Hu, Z., Shi, T., Cen, M., Wang, J., Zhao, X., Zeng, C., Zhou, Y., Fan, Y., Liu, Y., Zhao, Z., 2022. Research progress on lunar and martian concrete. Constr. Build. Mater. 343, 128117.
Huo, Y., Sun, H., Lu, D., Chen, Z., Yang, Y., 2022. Mechanical properties of concrete at low and ultra-low temperatures - a review. Journal of Infrastructure Preservation and Resilience 3 (1), 20.
Iranfar, S., Karbala, M.M., Shahsavari, M.H., Vandeginste, V., 2023. Prioritization of habitat construction materials on Mars based on multi-criteria decision-making. J. Build. Eng. 66, 105864.
Karacasulu, L., Karl, D., Gurlo, A., Vakifahmetoglu, C., 2023. Cold sintering as a promising ISRU technique: a case study of Mars regolith simulant. Icarus 389, 115270.
Karakoç, M.B., Türkmen, I., Maraş, M.M., Kantarci, F., Demirboğa, R., Toprak, M.U., 2014. Mechanical properties and setting time of ferrochrome slag based geopolymer paste and mortar. Constr. Build. Mater. 72, 283–292.
Krüger, M.E., Heisig, A., Hilbig, H., Eickhoff, H., Heinz, D., Machner, A., 2023. Effect of aluminum on the structure of synthetic alkali-silica gels. Cement Concr. Res. 166, 107088.
Lamaa, G., Duarte, A.P., Silva, R.V., de Brito, J., 2023. Carbonation of alkali-activated materials: a review. Materials 16 (8), 3086.
Lee, W., Van Deventer, J., 2002. The effects of inorganic salt contamination on the strength and durability of geopolymers. Colloids Surf. A Physicochem. Eng. Asp. 211 (2–3), 115–126.
Levchenko, I., Xu, S., Mazouffre, S., Keidar, M., Bazaka, K., 2021. Mars colonization: beyond getting there. Terraforming Mars 73–98.
Ma, S., Fu, S., Wang, Q., Xu, L., He, P., Sun, C., Duan, X., Zhang, Z., Jia, D., Zhou, Y., 2022. 3D Printing of damage-tolerant Martian regolith simulant-based geopolymer composites. Addit. Manuf. 58, 103025.
McKay, D.S., Allen, C.C., 1996. Concrete - a practical construction material for Mars. In: Engineering, Construction, and Operations in Space, pp. 566–570.
McSween, Jr H.Y., Keil, K., 2000. Mixing relationships in the Martian regolith and the composition of globally homogeneous dust. Geochem. Cosmochim. Acta 64 (12), 2155–2166.
Mills, J.N., Katzarova, M., Wagner, N.J., 2022. Comparison of Lunar and Martian regolith simulant-based geopolymer cements formed by alkali-activation for in-situ resource utilization. Adv. Space Res. 69 (1), 761–777.
Nana, A., Ngouné, J., Kaze, R.C., Boubakar, L., Tchounang, S.K., Tchakouté, H.K., Kamseu, E., Leonelli, C., 2019. Room-temperature alkaline activation of feldspathic solid solutions: development of high strength geopolymers. Constr. Build. Mater. 195, 258–268.
Nath, S.K., Kumar, S., 2019. Role of alkali concentration on reaction kinetics of fly ash geopolymerization. J. Non-Cryst. Solids 505, 241–251.

Nazari-Sharabian, M., Aghababaei, M., Karakouzian, M., Karami, M., 2020. Water on Mars - a literature review. Galaxies 8 (2), 40.
Neukart, F., 2024. Towards sustainable horizons: a comprehensive blueprint for Mars colonization. Heliyon 10, e26180.
Nurruddin, M.F., Sani, H., Mohammed, B.S., Shaaban, I., 2018. Methods of curing geopolymer concrete: a review. International Journal of Advanced and Applied Sciences 5 (1), 31–36.
Orosei, R., Lauro, S.E., Pettinelli, E., Cicchetti, A., Coradini, M., Cosciotti, B., Di Paolo, F., Flamini, E., Mattei, E., Pajola, M., 2018. Radar evidence of subglacial liquid water on Mars. Science 361 (6401), 490–493.
Panda, S., Nanda, A., Panigrahi, S.K., 2024. Potential utilization of waste plastic in sustainable geopolymer concrete production: a review. J. Environ. Manag. 366, 121705.
Reches, Y., 2019. Concrete on Mars: options, challenges, and solutions for binder-based construction on the red planet. Cement Concr. Compos. 104, 103349.
Sai Trivedi, S., Snehal, K., Das, B.B., Barbhuiya, S., 2023. A comprehensive review towards sustainable approaches on the processing and treatment of construction and demolition waste. Constr. Build. Mater. 393, 132125.
Scott, A.N., Oze, C., 2018. Constructing Mars: concrete and energy production from serpentinization products. Earth Space Sci. 5 (8), 364–370.
Scott, A.N., Oze, C., Tang, Y., O'Loughlin, A., 2017. Development of a Martian regolith simulant for in-situ resource utilization testing. Acta Astronaut. 131, 45–49.
Scott, A., Oze, C., Hughes, M.W., 2020. Magnesium-based cements for Martian construction. J. Aero. Eng. 33 (4), 04020019.
Shahsavari, M.H., Karbala, M.M., Iranfar, S., Vandeginste, V., 2022. Martian and lunar sulfur concrete mechanical and chemical properties considering regolith ingredients and sublimation. Constr. Build. Mater. 350, 128914.
Shao, R., Wu, C., Li, J., 2024. Innovative development of geopolymer-based lunar high strength concrete for sustainable extra-terrestrial construction using large-scale regolith simulants. Constr. Build. Mater. 450, 138707.
Shao, R., Wu, C., Li, J., 2025. Enhanced in-situ utilization of lunar simulant for fibre-reinforced high-performance concrete: mechanical properties and cost-effectiveness for lunar applications. Submitted to Journal of Materials Research and Technology.
Snehal, K., Sinha, P., Chaunsali, P., 2024. Development of waterless extra-terrestrial concrete using Martian regolith. Adv. Space Res. 73 (1), 933–944.
Szocik, K., Wójtowicz, T., Braddock, M., 2020. The Martian: possible scenarios for a future human society on Mars. Space Policy 54, 101388.
Thakur, R., Ghosh, S., 2011. Fly Ash Based Geopolymer Composites: Manufacturing and Engineering Properties. LAP.
Tran, H., Scott, A., 2017. Strength and workability of magnesium silicate hydrate binder systems. Constr. Build. Mater. 131, 526–535.
Triaud, A.H., de Wit, J., Klein, F., Turbet, M., Rackham, B.V., Niraula, P., Glidden, A., Jagoutz, O.E., Peč, M., Petkowski, J.J., 2024. Atmospheric carbon depletion as a tracer of water oceans and biomass on temperate terrestrial exoplanets. Nat. Astron. 8 (1), 17–29.
Trivedi, S.S., Sarangi, D., Das, B.B., Barbhuiya, S., 2023. Influence of multi-stage processing and mechano-chemical treatments on the hydration and microstructure properties of recycled aggregate concrete. Constr. Build. Mater. 409, 133993.
Vitse, J., Li, J., Boehme, L., Briers, R., Vandeginste, V., 2024. Martian regolith simulant-based geopolymers with lithium hydroxide alkaline activator. Buildings 14 (5), 1365.
Wan, L., Wendner, R., Cusatis, G., 2016. A novel material for in situ construction on Mars: experiments and numerical simulations. Constr. Build. Mater. 120, 222–231.
Wang, K., Tang, Q., Cui, X., He, Y., Liu, L., 2016. Development of near-zero water consumption cement materials via the geopolymerization of tektites and its implication for lunar construction. Sci. Rep. 6 (1), 29659.
Wang, J., Wu, D., Chen, K., Mao, N., Zhang, Z., 2024. Effect of Ca content on the synthesis and properties of FA-GGBFS geopolymer: combining experiments and molecular dynamics simulation. J. Build. Eng. 94, 109908.
Wu, C., Yu, Z., Shao, R., Li, J., 2024a. A comprehensive review of extraterrestrial construction, from space concrete materials to habitat structures. Eng. Struct. 318, 118723.
Wu, X., Zhou, X., Guo, C., Kang, D., Zhang, W., Lan, J., Fang, Z., 2024b. Behavior of hematite, magnetite, and reduced iron powder in geopolymers: effects of mechanical properties and reaction mechanism. J. Clean. Prod. 444, 141178.
Xie, J., Wang, J., Rao, R., Wang, C., Fang, C., 2019. Effects of combined usage of GGBS and fly ash on workability and mechanical properties of alkali activated geopolymer concrete with recycled aggregate. Compos. B Eng. 164, 179–190.
Xu, S., Yuan, P., Liu, J., Pan, Z., Liu, Z., Su, Y., Li, J., Wu, C., 2021. Development and preliminary mix design of ultra-high-performance concrete based on geopolymer. Constr. Build. Mater. 308, 125110.
Xu, S., Zheng, M., Yuan, P., Wu, P., Shao, R., Liu, Z., Liu, J., Wu, C., 2023. Experimental study of mechanical properties of G-UHPC against sodium sulfate attack at elevated temperature. Constr. Build. Mater. 396, 132387.
Yang, Z., Chen, Z., Zhu, H., Zhang, B., Dong, Z., Zhan, X., 2024. Efficient utilization of coral waste for internal curing material to prepare eco-friendly marine geopolymer concrete. J. Environ. Manag. 368, 122173.
Yu, T., Chen, J., Guo, H., Zhang, B., He, X., Zheng, A., Wang, Q., Yuan, P., 2023. Mechanical properties and microstructure of ground granulated blast furnace slag-based geopolymer reinforced with polyvinyl alcohol fibers. J. Mater. Cycles Waste Manag. 25 (3), 1719–1731.
Zamani, M.N., Ahmad Shah, M.S., Umar, S., Yahaya, N., Mukhlas, N.A., Kim, J.H.-J., Md Noor, N., 2024. The feasibility of in-situ resource utilisation binder systems for construction materials on Mars: a review. Adv. Space Res. 74 (3), 1535–1561.
Zhang, K., Xu, H., Kong, X., Zhang, C., Lu, H., He, D., 2023a. Study on the influence mechanism of micro-mechanical properties of heterogeneous geopolymer gels. J. Build. Eng. 76, 107164.
Zhang, H., Ai, J., Ren, Q., Zhu, X., He, B., Jiang, Z., 2023b. Understanding the strength evolution of alkali-activated slag pastes cured at subzero temperature. Cement Concr. Compos. 138, 104993.
Zhang, S.S., Wang, S., Chen, X., 2024. Understanding the role of magnesium ions on setting of metakaolin-based geopolymer. Cement Concr. Res. 177, 107430.
Zhou, S., Lu, C., Zhu, X., Li, F., 2021. Preparation and characterization of high-strength geopolymer based on BH-1 lunar soil simulant with low alkali content. Engineering 7 (11), 1631–1645.